Chemical Science

ROYAL SOCIETY OF CHEMISTRY

PERSPECTIVE

View Article Online
View Journal | View Issue

Cite this: *Chem. Sci.*, 2021, **12**, 3805

All publication charges for this article have been paid for by the Royal Society of Chemistry

All-in-one: a new approach toward robust and solution-processable copper halide hybrid semiconductors by integrating covalent, coordinate and ionic bonds in their structures

Xiuze Hei and Jing Li *

Conventional inorganic semiconductors are best known for their superior physical properties and chemical robustness, and their widespread use in optoelectronic devices. However, implementation of these materials in many other applications has been hindered by their poor solubility and/or solution-processability, a longstanding drawback that is largely responsible for issues such as high cost. While recent progress on hybrid perovskites, an important class of inorganic–organic hybrid materials, has shed light on the development of high-performance solution processable semiconductors, they rely heavily on toxic metals and generally suffer from framework instability. To address these issues, a new group of hybrid semiconductors based on anionic copper(I) halide and cationic organic ligands has been developed. These compounds are noted as All-In-One (AIO) structures as they consist of covalently bonded anionic CuX inorganic modules that form both coordinate and ionic bonds with cationic organic ligands. Studies demonstrate that framework stability and solution processibility of these materials are greatly enhanced as a result of such bonds. In the perspective, we highlight the development of this newly emerged type of materials including their crystal structures, chemical and physical properties and possible applications. The untapped potential that the AIO approach can offer for other hybrid families is also discussed.

Received 4th December 2020
Accepted 21st February 2021

DOI: 10.1039/d0sc06629j

rsc.li/chemical-science

1. Introduction

Inorganic–organic hybrid semiconductors represent an important class of crystalline functional materials. They are constructed by self-assembly of inorganic semiconductor motifs and organic ligands to form crystal structures of various dimensions. The integrated and enhanced properties, coupled with facile synthesis and systematic structural tunability make these materials particularly promising for applications in numerous energy and environment related fields, including but not limited to solid state lighting technology,[1–6] photovoltaics,[7–9] photodetection,[10–13] luminescent solar concentrators[14] and other renewable energy supplies.

One well-studied class of hybrid semiconductors is hybrid perovskites. While conventional inorganic semiconductors are best known for their superior electrical, optical and transport properties, along with structural robustness, one of the main advantages of hybrid perovskites is their excellent solubility and solution-processability.[15–17] The recent progress on hybrid perovskites has shed light on the development of solution-processable, cost-effective and large-area devices with high-performance.[18–21] Screen printing, slot-die coating, spin/spray coating and other methods have been developed to fabricate intermediate-sized perovskite-based solar cell modules on the scale of tens of square centimeters.[22] However, perovskite-based hybrid materials rely heavily on toxic elements and are generally lack of resistance towards moisture, heat and harsh environment. To address these issues, a new hybrid material family has recently been developed. These compounds consist of covalently bonded anionic copper(I) halide (CuX) inorganic modules that form coordinate and ionic bonds with cationic organic ligands, designated as All-In-One (AIO) structures. Note that all AIO-type compounds are composed of cuprous or Cu(I) ions. Due to different electron configurations of Cu(II) (d^9) and Cu(I) (d^{10}), hybrid cupric halides have very different properties from those of hybrid cuprous halides, and will not be included in this Perspective. The investigation into CuX-based inorganic–organic hybrid semiconductors can be dated back to 1970s.[23] Since then a large number of CuX-based hybrid structures have been reported in the Cambridge Crystallographic Data Centre (CCDC) database. These compounds can be classified into three sub-groups based on the nature of the chemical bonds (Scheme 1): type I structures are constructed of both charge-neutral inorganic CuX modules and organic ligands, which form coordinative bonds;[1,24–27] type II structures are built upon cationic ligands and anionic inorganic modules *via* pure ionic bonds;[5,28] The newly emerged type III structures are

Department of Chemistry and Chemical Biology, Rutgers University, Piscataway, New Jersey 08854, USA. E-mail: jingli@rutgers.edu

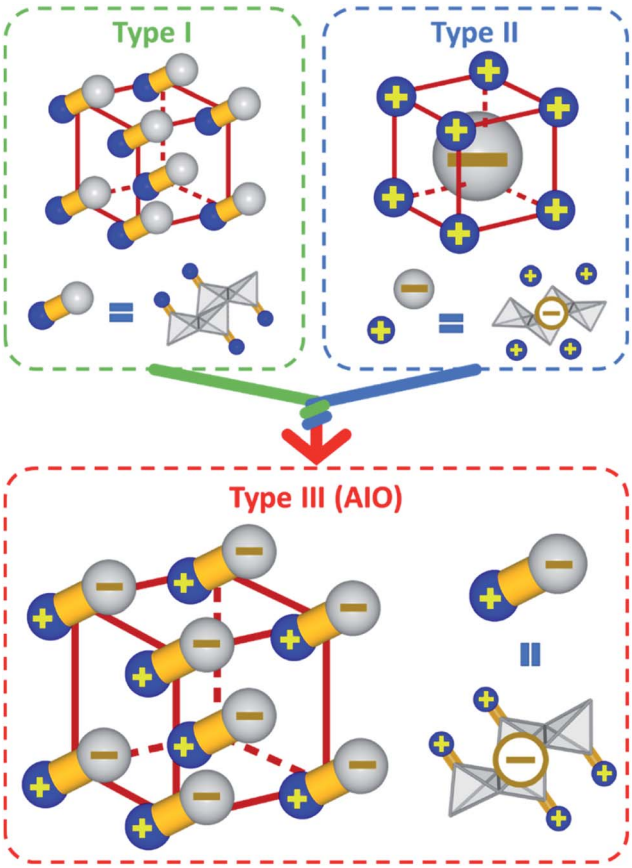

Scheme 1 Conceptual representation of type I, type II, and type III (AIO-type) structures. Color scheme: blue: organic ligand; gray: inorganic motif; yellow rod: coordinate bond. Type I structures are coordinate compounds made of Cu–L dative bonds only. Type II structures are ionic compounds built upon ionic bonds only. Type III structures are AIO compounds processing both ionic and dative bonds.

a combination of type I and type II structures, in which both inorganic and organic components are ionic (more specifically, cationic ligands and anionic inorganic modules) and also form coordinative bonds. Type III compounds are noted as AIO-type structures since all three types of chemical bonds, namely covalent bonds, coordinative bonds and ionic bonds, coexist in this type of compounds.[3,29–32] One should point out that there are some examples of hybrid CuX structures made of cationic inorganic modules and anionic ligands.[33] These compounds are essentially coordination polymers, and are excluded from the AIO family.

Most of the CuX(L) hybrid compounds reported to date belong to type I and type II structures. While type I compounds exhibit interesting and tunable properties and demonstrate high photoluminescence (PL) efficiency similar to perovskites,[3,5,34] major drawbacks include poor solution processability and/or instability. Type II compounds, on the other hand, often have limited structural tunability and relatively low PL efficiency. These deficiencies severely limit their applications in optoelectronic devices. The AIO-type structures, however, are designed to overcome these problems. Integration of coordinate bonds (as in type I compounds) and ionic bonds (as in type II compounds) in a single crystal lattice gives rise to a new structure type that possesses unique bonding characteristics and that inherits all the good features of both type I (*e.g.* bandgap tunability, strong luminescence) and type II (*e.g.* high solubility and framework stability) compounds described above. Such a desirable and unique bonding mode renders the AIO-type compounds a promising material class suitable for solution-processed fabrication of low-cost thin-film devices which would generally not be possible with type I or type II compounds. The AIO approach may also serve as a general and powerful tool for the development of many other solution-processable hybrid material families. Interest in this material class also originates from the strong interplay of the organic and inorganic motifs in their crystal lattices.[29–32,35] By suitable combination of these building blocks, one can fine tune their structural, electronic, optical and chemical properties systematically to achieve targeted performance. Therefore, featuring electronic/optical tunability, air/moisture/thermal stability, strong photoluminescence and excellent solution processability, AIO-type structures have already demonstrated superior performance as eco-friendly lighting phosphors and luminescent solar concentrators.[3,5,29–31,36] Most recent studies also suggest their potential use in other energy-related devices, such as LEDs, photovoltaics and photodetectors.

Type I and type II CuX-based hybrid structures have been discussed extensively in a number of previously published review articles and, therefore, will not be the subject of this article.[3,24,34,37,38] This Perspective aims to provide a timely overview of the recent advances on type III (AIO-type) compounds, with a focus on the structure types, important properties and structure–property correlation. We will also briefly discuss the possible applications, main challenges and future outlook of these materials and their derivatives.

2. Crystal structures of AIO-type compounds

As stated above, the AIO-type compounds can be considered as a combination of type I and type II CuX-based hybrid structures by integrating covalent, coordinative and ionic bonds into a single crystal lattice. So far, over 30 AIO-type CuX(L) compounds have been designed and synthesized, and their structures range from molecular species (zero-dimension, 0D) to one-dimensional (1D) chains and two-dimensional (2D) networks. The organic ligands are designed to be either aliphatic or aromatic and contain both cationic centers (*e.g.* quaternary N or P) and active binding sites for subsequent coordination to Cu atoms. The cationic ligands are generally synthesized by alkylation of selected ligands that contain both active copper–ligand binding sites and alkylation site (*e.g.*, triethylenediamine, benzotriazole derivatives). This ensures the formation of cationic centers that do not interfere with the direct coordination of the ligands to the copper metals. The active binding sites are typically N, S, or P atoms, which can form strong coordinative/dative bonds with Cu atoms (Fig. 1

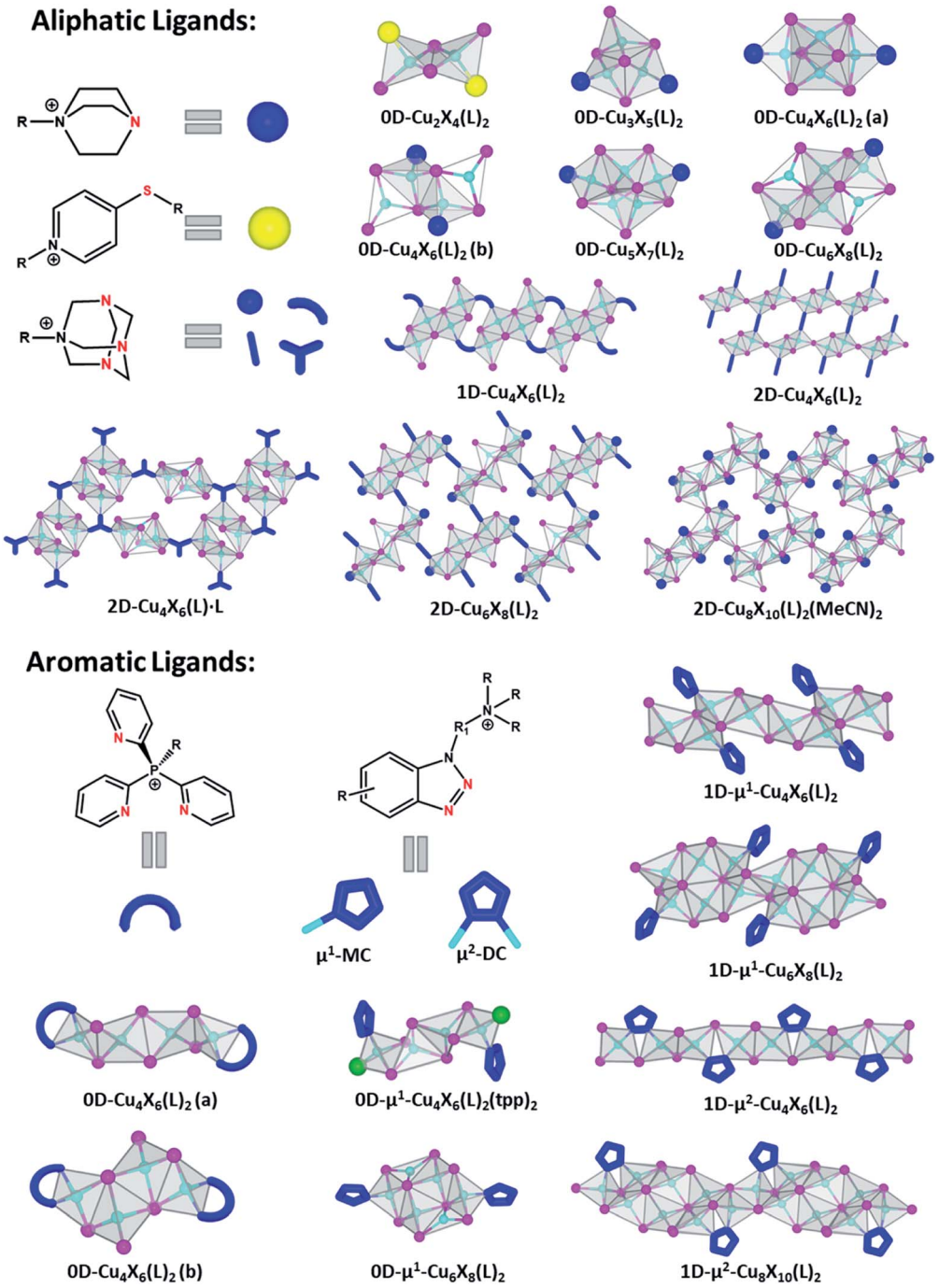

Fig. 1 Representative structures of AIO-type compounds. Color scheme: Cu, cyan; X, purple; P, green. Active coordination sites of the ligands (N and S) are marked in red.

and Table 1). Depending on the orbital hybridization of the coordinative atoms, sp^3 for aliphatic ligands and sp^2 for aromatic ligands, the AIO hybrid compounds synthesized may follow different emission mechanisms which will be discussed in a later section.

2.1. AIO-type compounds based on aliphatic ligands

The first group of the AIO-type structures were discovered in 2017,[29] of which seven different molecular species are based on aliphatic ligands. The Cu–N distances in these compounds are similar to the typical Cu–N bond lengths found in type I CuX based hybrid structures (2.0–2.2 Å).[25,39] The Cu atoms are tetrahedrally coordinated either to four iodine atoms or to a combination of four iodine atoms and ligands, and the coordination number of I atoms ranges from 1 to 4. While all six ligands share similar configurations, namely one-side alkylated triethylenediamine, five different $Cu_mI_{m+2}^{2-}$ clusters ranging from dimer ($Cu_2I_4^{2-}$) to hexamer ($Cu_6I_8^{2-}$) are obtained.

Table 1 Summary of important physical properties of AIO compounds at room temperature

Compound	Bandgap, eV	λ_{em}, nm	Emission color	IQY, % (λ_{ex}, nm)	T_D, °C	Ref.
Aliphatic ligand based AIO structures						
0D-Cu_3I_5(*bz-ted*)$_2$	3.0	560	Yellow	75 (360)	270	29
0D-Cu_4I_6(*3-Cl-pr-ted*)$_2$	3.1	540	Green-yellow	92 (360)	270	29
0D-Cu_4I_6(*pr-ted*)$_2$	3.1	535	Green	92 (360)	280	29
Cu_4I_6(*pr-ted*)$_2$/PVP ink	3.1	526	Green	98 (365)	270	36
0D-Cu_4I_6(*2-Br-et-ted*)$_2$	2.9	535	Green	75 (360)	280	29
0D-Cu_5I_7(*i-pr-ted*)$_2$	3.1	575	Orange	70 (360)	310	29
0D-Cu_6I_8(*bu-ted*)$_2$	3.0	530	Green	90 (360)	300	29
0D-Cu_2I_4(*mtp*)$_2$	2.3	555	Yellow	61 (360), 52 (450)	210	29
1D-Cu_4I_6(*Pr-hmta*)$_2$	3.5	510 (298 K), 512, 583 (77 K)	Yellow	16 (300)	160	32
1D-Cu_4I_6(*Ppg-hmta*)$_2$	3.0	470 (298 K), 483, 550 (77 K)	Cyan	50 (300)	180	32
2D-Cu_4I_6(*Me-hmta*)$_2$	3.4	430 (298 K), 430, 570 (77 K)	Deep blue	26 (300)	230	32
2D-Cu_8I_{10}(*Me-hmta*)2(*MeCN*)$_2$	3.3	497	Cyan	10 (300)	140	32
2D-[*Et-hmta*][Cu_4I_6(*Et-hmta*)] · *MeCN*	2.3	570	Yellow	78 (300)	105	32
2D-Cu_6I_8(*Pr-hmta*)$_2$(*MeCN*)$_2$	3.5	630	Orange-red	56 (300)	145	32
Aromatic ligand based AIO structures						
0D-Cu_4I_6(*tpp*)$_2$(*bttmm*)$_2$	2.5	540	Green-yellow	90 (360), 71 (450)	200	29
0D-Cu_4I_6(*tpp*)$_2$(*btmdem*)$_2$	2.4	545	Green-yellow	64 (360), 42 (450)	180	29
0D-Cu_6I_8(*btmdb*)$_2$	2.4	540	Green-yellow	70 (360), 51 (450)	200	29
0D-Cu_4I_6(*Pr-tpp*)$_2$	2.0	640	Red	1.1 (440)	250	35
0D-Cu_4I_6(*Bu-tpp*)$_2$	2.0	623	Orange-red	1.0 (440)	230	35
0D-Cu_4I_6(*Bn-tpp*)$_2$	2.0	649	Red	3.5 (440)	225	35
1D-μ^1-Cu_4I_6(*btdmem*)$_2$	2.6	550	Green-yellow	25 (360), 21 (450)	190	30
1D-μ^1-Cu_6I_8(*btdmpm*)$_2$	2.5	650	Red	29 (360), 24 (450)	193	30
1D-μ^2-Cu_8I_{10}(*bttmb*)$_2$	2.65	528	Green	80 (360), 64 (450)	245	30
1D-μ^2-Cu_4I_6(*bttmpe*)$_2$	2.45	552	Green-yellow	70 (360), 64 (450)	235	30
1D-μ^2-Cu_4I_6(*5-F-bttmp*)$_2$	2.2	615	Orange-red	53 (360), 44 (450)	225	30
1D-μ^2-Cu_4I_6(*5-m-bttmp*)$_2$	2.45	596	Orange-red	85 (360), 76 (450)	225	30
1D-μ^2-Cu_4I_6(*5,6-dm-bttmp*)$_2$	2.5	570	Yellow-orange	68 (360), 65 (450)	235	30
1D-μ^2-Cu_4I_6(*bttmmp*)$_2$	2.4	553	Green-yellow	53 (360), 40 (450)	211	30
1D-μ^2-Cu_4I_6(*bttme*)$_2$	2.45	585	Orange	69 (360), 57 (450)	210	31
1D-μ^2-Cu_4Br_6(*bttme*)$_2$	2.5	615	Orange-red	56 (360), 44 (450)	220	31
1D-μ^2-Cu_4Br_6(*bttmpe*)$_2$	2.5	600	Orange-red	69 (360), 60 (450)	250	31

Additionally, some CuX clusters have the same composition but different structures. For example, two different $Cu_4I_6^{2-}$ clusters are obtained with different ligands. On the other hand, structures constructed by identical inorganic clusters but different ligands are also obtained. For instance, reactions of CuI with either *pr-ted* or *2-Br-et-ted* both afford the same hourglass-shaped cluster. These examples add another degree of structural diversity to this material group. It is worth noting that Cu···Cu distances in all aliphatic ligand based AIO structures are relatively short, from 2.56 to 2.72 Å, which are shorter than twice vdW radius of Cu (2.80 Å).[40] This may be indicative of cuprophilic interactions which are the main reason for cluster-centered (CC) optical emission and will be discussed in detail in the next section.

The success in the synthesis of discrete AIO-type molecular species has inspired continuous effort in constructing extended networks of AIO structures based on $Cu_mX_m^{2-}$ molecular clusters and ligands with multiple binding sites. Using *N*-monoalkylated hexamethylenetetramine salts as ligands that contain three active N binding sites, the AIO family was successfully expanded to include a series of 1D–2D structures. Six new AIO compounds with three unique halocuprate(I) motifs have been recognized and the organic cationic ligands display diverse coordination modes (*i.e.* N-terminal, *N*,*N*′-bridging and *N*,*N*′,*N*″-bridging). Although the chemical structures and topology of these compounds are largely affected by the nature of substituent R groups in the monoalkylated ligands, the Cu–N bond lengths, Cu–I bond lengths and Cu···Cu distances are comparable with those in the 0D AIO molecular structures.

2.2. AIO-type compounds based on aromatic ligands

Six different AIO-type molecular species based on aromatic ligands have been reported so far. They adopt three different inorganic CuX modules, as those in 0D-$Cu_4X_6(L)_2$(a), 0D-$Cu_4X_6(L)_2$(b), and μ^1-0D-$Cu_6X_8(L)_2$ (Fig. 1).[29,35] All of these 0D-AIO compounds are synthesized by using relatively bulky ligands, for example, butyl-tris(2-pyridyl)phosphonium iodide (*Bu-tpp*) and *N*-((1*H*-benzo[*d*][1,2,3]triazol-1-yl)methyl)-*N*,*N*-dibutylbutan-1-aminium iodide (*btmdb*), which effectively separate the inorganic modules from each other. Interestingly, these 0D AIO compounds generally have much longer Cu···Cu distances (3.01–3.36 Å) than those in the aliphatic ligand based 0D AIO compounds (2.56–2.74 Å). The size of alkyl substituent in the ligands appears to be important in the formation of AIO-

type compounds.[35] For example, *Pr-tpp*, *Bu-tpp* and *Bn-tpp* (Bn = benzyl group) lead to AIO-type structures, while *Me-tpp* directs to an ionic complex.

Most recently, by using benzotriazole derived cationic ligands with deliberately designed coordination modes and active sites, we have succeeded in expanding the dimensionality of the inorganic module from molecular clusters (0D) to infinite chains (1D) and achieving a series of 1D-AIO compounds with enhanced framework stability and photoluminescence quantum yield (PLQY).[30] Since each ligand has two N atoms that are available to bind with Cu, two different coordination modes are possible which results in four different $Cu_mI_{m+2}^{2-}$ anionic chains. 1D-μ^1-$Cu_4I_6^{2-}$ (type-1) and 1D-μ^1-$Cu_6I_8^{2-}$ chains (Fig. 1) adopt the monocoordination mode (μ^1-MC), in which only one N atom in each ligand molecule forms bond with Cu atom. Two remaining chains, 1D-μ^2-$Cu_4I_6^{2-}$ (type-2) and 1D-μ^2-$Cu_8I_{10}^{2-}$ adopt the dicoordination mode (μ^2-DC), where both N atoms from each ligand are coordinated to Cu atoms and form a five-member ring with a bridging I.

The main reason of such different coordination behaviour was found to be the alkyl chain length of the cationic ligands. When the distance between the benzotriazole and ammonium cationic center is very short, the electron density of the middle N atoms (N1, Fig. 2a) can be substantially reduced due to the inductive effect,[41] and thus inhibits the Cu–N1 coordination, leading to the μ^1-MC structures (Fig. 2b). In the μ^2-DC structures with elongated alkyl chain, such inductive effect is reduced so that both N atoms can coordinate with Cu atoms to form the five-member ring (Fig. 2b). While steric effect of the short-chain ligands may also play a role in the coordination mode, such effect is relatively minor.[42,43] Further studies on the coordination affinity of the ligands in μ^2-DC structures suggest their structural directing effect.[31] As mentioned above, N1 is affected more by the NR_4^+ inductive effect than N2 and thus forms longer Cu–N1 bonds than Cu–N2 bonds. This length difference causes distortion to the 1D-Cu_mX_{m+2} chain and leads to a zig-zag form with a "*cis*" orientation of ligands. The difference between the two Cu–N bonds becomes negligible when the inductive effect is significantly reduced with longer alkyl chains, resulting in a "flattened" inorganic backbones and allow a "*trans*" orientation of the ligands (Fig. 2b).

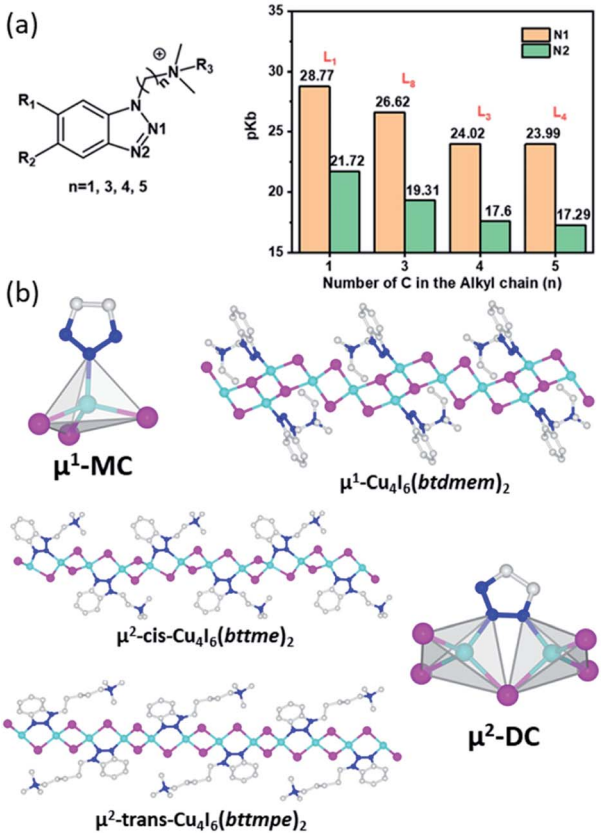

Fig. 2 (a) Ligand structures used to calculate pk_b values of N1 and N2 (left) and the calculated results in selected ligands with different alkyl chain length (right). Reproduced with permission from ref. 31. Copyright 2020, American Chemical Society. (b) Illustration of μ^1-MC, μ^2-DC modes and ligand orientations with representative hybrid structures. Color scheme: Cu, cyan; I, purple; N, blue; C, Gray.

3. Important properties of AIO compounds

3.1. Solubility and solution processability

Conventional inorganic semiconductors such as Si[44] and GaN[45] are well known for their superior physical properties and stability, and thus currently dominate the high-end device markets.[46] However, the inherent limitations of these semiconductors with respect to stringent material/processing requirements (*e.g.* high purity, high temperature or high vacuum) and their poor solution processability not only result in high cost for device fabrications but also hamper their use in other applications.[47] It is well recognized that solution processed semiconductors may become a new paradigm in optoelectronic device industries.[48–50] While cost-effective and high-quality film fabrication by blade coating, inkjet printing or other existing printing technologies have been developed for various solution processable semiconductor materials,[50–52] such materials are largely limited to pure ionic compounds and organic polymers that may not be the best candidates for certain applicaitons.[11,53,54] Colloidal quantum-dot based materials are examples of solution-processable covalently bonded network structures however their synthesis is often challenging and associated with high cost.[55–59]

The AIO approach may serve as a general and powerful tool for the design of solution processable hybrid materials containing covalent/coordinate bonds, including but not limited to copper halide based systems.[30] Despite that AIO-type compounds are coordinate networks and often contain infinite inorganic modules (*e.g.* 1D $Cu_mI_{m+2}^{2-}$ chains and 2D-Cu_8I_{10} layer), they demonstrate remarkably high solubility in DMSO and other polar aprotic solvents, comparable with those of common inorganic salts.[60] This property is distinctly different from most of type I charge neutral Cu_mI_m structures, especially those with extended networks, that are totally insoluble in any common organic and inorganic solvents[1,3,60] (Fig. 3a and b).

Taking compound [1D-Cu_6I_8(*btdmpm*)$_2$] as an example, 1 ml of DMSO can readily dissolve about 350 mg of the sample within 5 min at room temperature under ultrasonication (Fig. 3e). Upon addition of antisolvent such as methanol or slow cooling of the preheated saturated DMSO solution, the compound can be recovered/recrystallized. Such behavior has been observed for all other 1D-AIO compounds. A simple drop-cast or spin-coat the 1D-AIO/DMSO solution can afford high quality thin films on either glass substrates or soft fabrics (Fig. 3c and d). Using the 0D-Cu_4I_6(*pr-ted*)$_2$ cluster first synthesized by us,[29] Yao and co-workers successfully prepared a highly luminescent AIO/polymer ink.[36] The Cu_4I_6(*pr-ted*)$_2$/PVP ink was facilely fabricated *via* a one-pot solution synthesis, by adding CuI and *pr-ted* into a polyvinylpyrrolidone (PVP) ethanol solution. The reaction afforded a Cu_4I_6(*pr-ted*)$_2$/PVP nanoparticle composite with an average diameter around 100 nm. High quality painting of a bamboo tree and a thin film deposited on a large rectangular quartz substrate (9 cm × 4.5 cm) using the as-synthesized ink are shown in Fig. 3f. The high quality of the film was confirmed by both cross-sectional SEM and AFM analysis (Fig. 3g).

The solvation behavior of the AIO-type compounds is found similar to that of hybrid perovskite structures. For example, hybrid perovskite (MA)PbI_3 exhibits much higher solubility in DMSO than PbI_2. Due to the strong interaction between DMSO and the inorganic module, as well as the presence of iodide ions from MAI, the perovskite structures undergo complexation in DMSO to generate soluble trinuclear plumbate $(MA^+)_2[(PbI_3^-)_2PbI_2]\cdot(DMSO)_2$, thereby giving rise to a remarkable solubility.[61–63] In an analogous manner, all 1D-$Cu_mI_{m+2}(L)_2$ compounds show enhanced solubility in DMSO than CuI and especially neutral CuI(L) compounds, which may be attributed to a similar complexation process.[30] ^{1}H NMR spectroscopy was used to confirmed this hypothesis.[31] The spectra of the DMSO solutions of AIO compounds show characteristic peaks of the free ligands but with some shifts. Careful analysis of the differences suggests that the dissolved species are primarily small fragments composed of CuX clusters remaining coordinated to the ligands *via* Cu–N dative bonds.

The solvation behavior of 0D-AIO molecular species in MeCN was also studied by Alexander A. and co-workers using electrospray ionization mass spectrometry (ESI-MS) and NMR

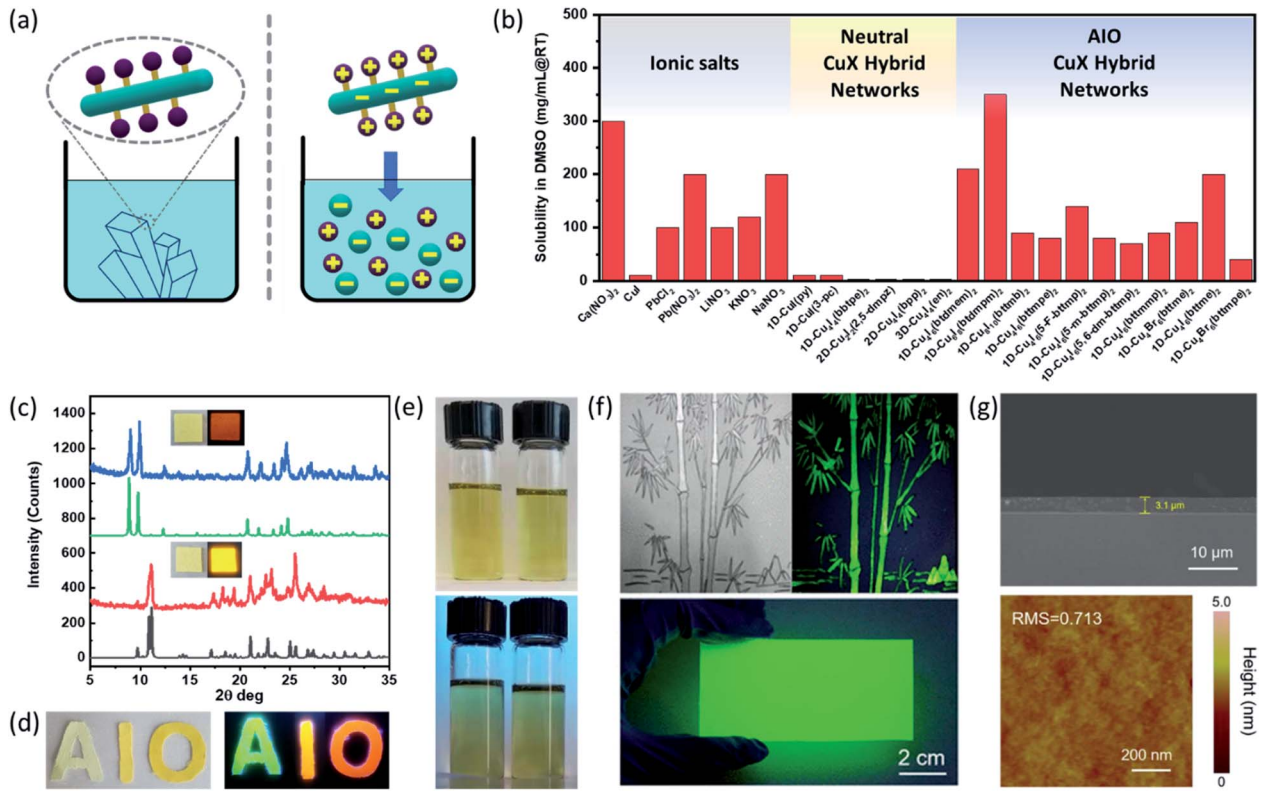

Fig. 3 (a) Structure similarity and solubility difference of charge-neutral 1D-CuI(L) (Left, Insoluble) and 1D-AIO-(Cu_mx_{m+2})L_2 (right, soluble) compounds. (b) Solubility data for common inorganic salts (left), neutral CuI(L) networks (middle) and 1D-AIO-(Cu_mx_{m+2})L_2 compounds (right). (c) PXRD patterns of thin films of AIO-type extended networks (red and blue) and corresponding simulated patterns from single crystal data (black and green). Inset: optical images of thin films of 1D-μ^1-Cu_6I_8(*btdmpm*)$_2$ and 1D-μ^2-Cu_4I_6(*5-m-bttmp*)$_2$ under daylight (left) and 365 nm UV light (right). (d) Selected 1D-AIO compounds coated on soft fabric (left: under daylight; right: under ultraviolet light source). (e) Optical images of 200 mg 1D-μ^1-Cu_6I_8(*btdmpm*)$_2$ (left) and 1D-μ^2-Cu_4I_6(*5-m-bttmp*)$_2$ (right) dissolved in 3 ml DMSO under day light (top) and 365 nm UV light (bottom). (f) A picture painted by the 0D-Cu_4I_6(*pr-ted*)$_2$/PVP ink under natural light (top left) and 365 nm ultraviolet light (top right), respectively and a large-area film deposited on glass substrate by a doctor-blade coating process (bottom). (g) Cross-sectional SEM image (top) and AFM image (bottom) of the as-fabricated 0D-Cu_4I_6(*pr-ted*)$_2$/PVP film. (a), (c)–(e) are reproduced with permission from ref. 30. Copyright 2020, American Chemical Society. (f)–(g) are reproduced with permission from ref. 36. Copyright 2020, American Chemical Society.

techniques. The results are consistent with those found for 1D-AIO structures.[35] Although the ESI-MS(−) spectra of both pure ionic hybrid structures and AIO structures share similar features, namely the characteristic peaks for $[Cu_nI_{n+1}]^-$ anions (n = 2 to 12), the ESI-MS(+) spectra clearly distinguish AIO compounds from ionic structures. Only the spectra of AIO structures exhibit dominating signals assigned to the $[(L)_3Cu_mI_{m+2}]^+$ cations (n = 4–9). The coordination of ligands to copper in the solution state was further confirmed by ^{1}H NMR spectra of dissolved AIO compounds. The signals of H-6 pyridine protons in solution down-shifted compared to those in free ligands. Additionally, it is worth to note that the non-equivalent pyridine protons in the solid state (only two out of three N_{py} atoms are bonded to Cu atoms) become undistinguishable in solution state, indicating the fast and repetitive "dissociation-association" processes of Cu–N_{py} bonds. Both the ESI-MS and NMR data suggest the significant influence by the nature of the parent complex (ionic or AIO).[35]

3.2. Chemical and thermal stability

Besides cost-effective facile synthesis and solution-based film processability, semiconductor materials must also possess high stability towards moisture, light, and heat in order to meet the requirement for practical applications.[5] Held by both ionic and coordinate bonds between the ligand and inorganic module, the AIO-type structures generally demonstrate significantly enhanced framework stability compared to those hybrid structures held by only coordinate bonds (*e.g.* neutral CuI(L) compounds) or solely ionic bonds (*e.g.* hybrid perovskites). All the AIO structures reported to date, including molecular species (0D) and extended networks (1D-2D), show good resistance towards heat. With a few exceptions, most of them do not decompose until above ~200 °C, with some exceeding 300 °C (Table 1). Additionally, both the aliphatic and aromatic ligand-based AIO structures exhibit excellent long-term photo-stability. For example, the internal quantum yield (IQY) values of 0D-AIO compounds [0D-Cu_4I_6(*pr-ted*)$_2$] and [0D-Cu_4I_6(*tpp*)$_2$(*bttmm*)$_2$] remained over 90% compared to their initial values, after being heated at 100 °C or under continuous UV (365 nm) irradiation for 20 days without any protection.[29] On the other hand, the neutral molecular compounds, [0D-Cu_2I_2(*py*)$_4$] and [0D-Cu_4I_4(*py*)$_4$], suffered from nearly 100% drop in their IQYs upon heating for merely 1 day, and these values were reduced by ~50% and ~80% at the end of the photostability experiment (Fig. 4b). The liquid ink made of 0D-Cu_4I_6(pr-ted)$_2$/PVP remains nearly unchanged and strongly luminescent even after 10 days. To further improve the stability of these AIO compounds, several approaches have been made as illustrated in Fig. 4a and briefly discussed below.

The first approach is to select organic ligands with higher connectivity to form multidentate structures (Fig. 4a, approach 1). In the case of $Cu_4I_6^{2-}$ based 0D-AIO clusters, substituting two monodentate ligands with one bidentate ligand generally leads to a considerable increase in the decomposition

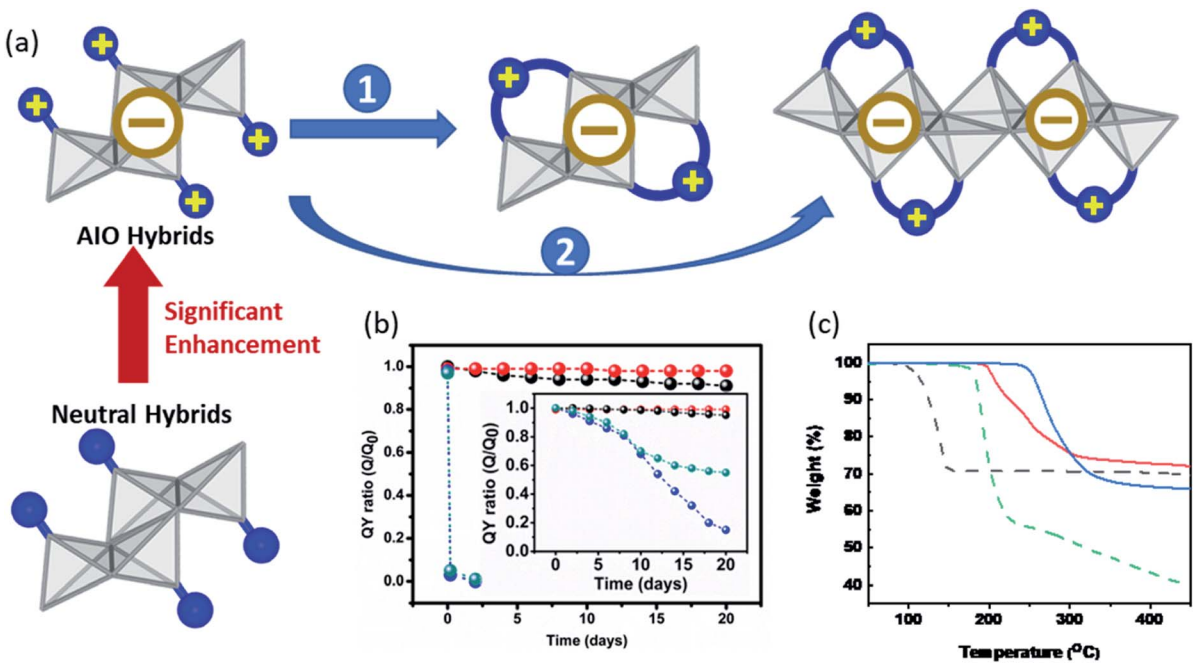

Fig. 4 (a) Schematic illustrating different approaches to enhance the stability of AIO-type compounds. Gray polyhedra:inorganic motifs; blue ball:organic ligands. (b) Plots of IQY ratios (Q_0 and Q are IQY values measured before and after heating the sample at 100 °C in air as a function of time) for the selected neutral 0D-Cu_mI_m(L)$_4$ and 0D-AIO-Cu_mI_{m+2}(L)$_2$ cluster compounds. Inset is the plots of ratios of the IQY values after and before exposing to UV (365 nm) light as a function of time. Blue: 0D-Cu_2I_2(*py*)$_4$, green: 0D-Cu_4I_4(*py*)$_4$, red: 0D-Cu_5I_7(*i-pr-ted*)$_2$, black: 0D-Cu_6I_8(*btmdb*)$_2$. Reproduced with permission from ref. 29. Copyright 2017, American Chemical Society. (c) TG plots of staircase chain-like 1D-CuI(*py*) (dotted black), 0D-Cu_4I_6(*tpp*)$_2$(*bttmm*)$_2$ (dotted green), 1D-μ^1-Cu_6I_8(*btdmpm*)$_2$ (red) and 1D-μ^2-Cu_4I_6(*5,6-dm-bttmp*)$_2$ (blue). Reproduced with permission from ref. 31. Copyright 2020, American Chemical Society.

temperature, as a result of chelate effect.[64] 0D-Cu_4I_6(*Bu-tpp*)$_2$ serves as a good example. It demonstrates an enhanced thermal stability by 50 °C compared to the 0D-Cu_4I_6(*tpp*)$_2$(*btmdem*)$_2$, which consists of exact the same inorganic structure but four monodentate ligands.

The other approach to enhance the framework stability is to build extended networks (Fig. 4a, approach 2). It has been proven that generally the thermal- and photo-stability of neutral CuI(L) hybrid structures follow the following trend: 0D < 1D < 2D < 3D,[39] which is applicable to the AIO-type structures as well. All 1D-AIO structures built on benzotriazole derivatives are stable up to at least 190 °C, notably higher than the 0D-AIO clusters made of the same ligand (Fig. 4c). It is worth noting that the μ^2-DC structures are more robust than μ^1-MC structures, as the former has a higher connectivity than the latter (see approach 1). The strength of Cu–N coordinate bond also plays an important role in the stability. As described in the previous sections, the Lewis basicity and electron donating ability of the coordination-available N atoms in the benzotriazole-based ligands (N1 and N2, Fig. 2a) can be largely affected by their distances from the cationic centers, thus affording Cu–N coordinate bonds with different strength. The thermal stability of AIO compounds that share the same inorganic motifs follow the same trend as the binding strength of their Cu–N dative bonds, confirmed by the thermogravimetric (TG) analysis and theoretical calculations.

3.3. Optical properties

As a combination of type I and type II CuX based hybrid materials, the AIO structures also exhibit intriguing optical properties, including strong absorption of energy, intensive luminescence, and systematic tunability. Employing numerous experimental and theoretical methods, we and others have thoroughly investigated the important optical properties and luminescence mechanisms of these materials.

As shown in Table 1 and Fig. 5a, intense photoluminescence that covers the entire visible spectrum has been achieved (Fig. 5a) for these compounds. Like the extensively studied type I neutral CuX-based hybrid structures, the emission mechanisms of AIO-type compounds include metal-to-ligand charge transfer (MLCT), halide-to-ligand charge transfer (XLCT) and cluster-centered charge transfer (CC), or combinations of these, which strongly correlates to the Cu⋯Cu distances within the structure (Fig. 5b). It has been demonstrated that Cu⋯Cu distance, as an indicator of cuprophilic interaction, plays a vital role in the CC transitions. Compounds with strong CC transitions usually have Cu⋯Cu distance less than 2.80 Å (twice of the vdW radius of Cu).[65–67] On the other hand, MLCT and XLCT or (M + X)LCT based emissions are typically observed in structures that are lack of strong cuprophilic interaction.[1,25,29–31,35,39,60,68] Interestingly, when the Cu⋯Cu distance falls to the borderline, both pathways, namely CC and (M + X)LCT, can occur simultaneously and show responsive dual emissions as a function of excitation energy and/or temperature.[32]

Generally, AIO compounds composed of aliphatic ligands have shorter Cu⋯Cu distances than those made of aromatic ligands and, hence, typically show pure CC emission mechanism. All the aliphatic ligand based 0D-AIO structures reported so far follow this emission mechanism and their emission energies are mainly determined by the inorganic cores with negligible ligand effect. These compounds usually show large stokes shift. It is worth noting that preliminary study on the (limited number of) aliphatic ligand based AIO extended network structures reveals that structural rigidity may also play a role in the excited state configuration. It has been proven both theoretically and experimentally that when the CuX based hybrid materials are being promoted to the CC excited state, decrease in Cu⋯Cu distance may occur.[69,70] As a result, flexible frameworks can accommodate the associated structure change and thus enhance the CC emission, while rigid frameworks tend to diminish such changes. Electronic state calculations on the aliphatic ligand based AIO extended networks (with an average Cu⋯Cu distance of ~2.80 Å) show that both inorganic and organic motifs contribute to the CBM, suggesting both CC and (M + X)LCT emission pathways are possible.[32] However, depending on the Cu⋯Cu distances and structural rigidity, one or both processes may play a dominating role. Structures with relatively short average Cu⋯Cu distances and high flexibility exhibit comparable emissions from both pathways.

Careful analysis on the AIO-type structures that exhibit chromism behavior *via* temperature- and excitation-dependent solid state photoluminescence spectroscopy suggests that the two pathways, namely ^{3}CC and ^{3}(M + X)LCT, could be poorly coupled and higher energy is required to populate the higher laying state (Fig. 5c).[32] This was confirmed by the Density Function Theory (DFT) calculations. The valence band maximum (VBM) of the copper iodide AIO compounds is primarily composed of the inorganic atomic states, specifically Cu 3d and I 5p orbitals, and the conduction band minimum (CBM) is populated either by organic components (*i.e.* C and N 2p orbitals) or a combination of organic and inorganic components. In the latter case, a small energy difference was observed between their energy levels, suggesting the poor coupling of the two excitation states as indicated in Fig. 5c. This finding is also consistent with the behavior observed in some type I CuX hybrid structures with similar average Cu⋯Cu distances.[71–73] Therefore, the relative intensity of higher laying state based emission can be tuned by varying the energy applied to the process (*e.g.* temperature or excitation wavelength), resulting in responsive dual emitters towards temperature and excitation energy.[32] For example, the emission color of 1D-Cu_4I_6(*Pr-hmta*)$_2$, with average Cu⋯Cu distance of 2.80 Å and relatively flexible structures, can be smoothly adjusted from cyan to orange-red by changing excitation wavelength from 260 to 380 nm or lowering the temperature from 300 K to 77 K. On the other hand, AIO compound 2D-Cu_6I_8(*Pr-hmta*)$_2$(*MeCN*)$_2$ constructed with same ligand but have longer average Cu⋯Cu distance (3.06 Å) and higher structural rigidity only displays one emission band within 77–300 K window, which may be attributed to the destabilized ^{3}CC state caused by longer average Cu⋯Cu distances and higher rigidity.

The AIO structures based on aromatic ligands usually have longer Cu⋯Cu distances and thus, typically follow the (M + X)

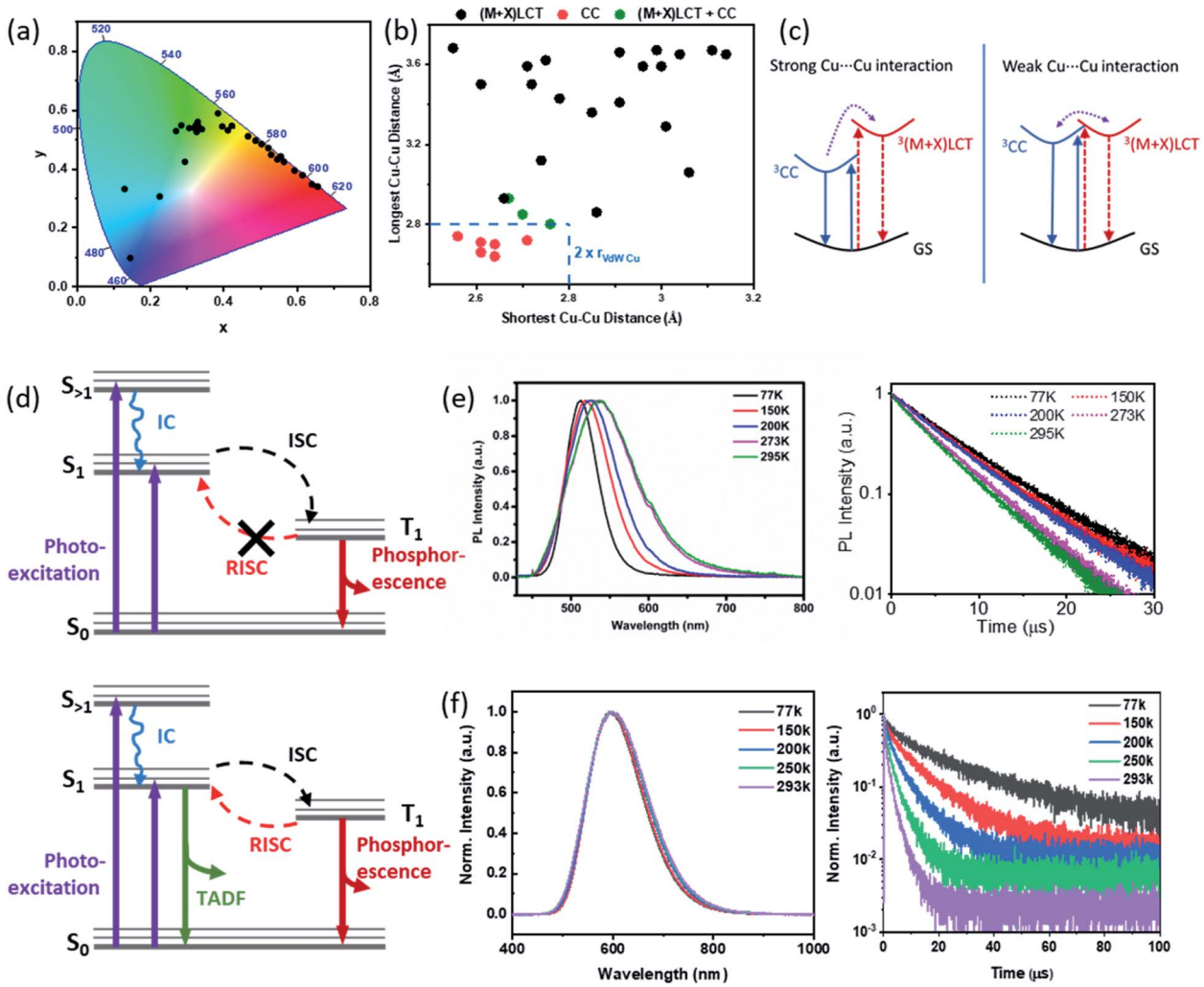

Fig. 5 (a) Color chromaticity of all AIO-type compounds reported to date. (b) Correlation between the Cu···Cu distances in the AIO-type compounds and their emission mechanisms. (c) Qualitative energy diagrams for the ^{3}CC and^3(M + X)LCT excited states for compounds with strong Cu···Cu interaction (left) and weak Cu···Cu interaction (right). GS, ground state. Reproduced with permission from ref. 32. Copyright 2020, American Chemical Society. (d) Energy diagrams of compounds indicating phosphorescence (upper) and compounds indicating TADF and phosphorescence emission processes (bottom). (e and f) Normalized emission spectra (left) and luminescence decay profiles (right) at various temperatures for 0D-Cu_4I_6(*pr-ted*)$_2$ and 1D-μ^2-Cu_4I_6(*5,6-dm-bttmp*)$_2$. (e) Reproduced with permission from ref. 29. Copyright 2017, American Chemical Society. (f) Reproduced with permission from ref. 30. Copyright 2020, American Chemical Society.

LCT emission mechanism. The CBM of these compounds is populated mainly by the lowest unoccupied molecular orbital (LUMO) of ligands.[3] Spectroscopic studies demonstrate that their bandgaps are generally in trend with the calculated ligand LUMO energies. Therefore, their bandgaps and emission energies can be systematically regulated by using ligands with appropriate LUMO energies. For example, by adding electron withdrawing group (EWG) or electron donating group (EDG) to the ligand, the original LUMO can be stabilized or destabilized to alter its energy level and consequently the bandgap of the resulting hybrid compounds.[74] Therefore, the bandgap of the AIO compounds, which share exactly the same 1D-μ^2-$Cu_4I_6^{2-}$ backbone, can be tuned from 2.2 to 2.5 eV, following the same trends as the LUMO energies of free ligands calculated by density functional theory (DFT) and thus lead to emission range from 570 to 615 nm.[30]

Thermochromic behavior has been observed in some AIO compounds that undergo CC emission mechanism. The 0D-Cu_4I_6(*pr-ted*)$_2$ shows a 30 nm blue shift in its emission energy accompanying with a peak width narrowing as the temperature is lowered from 298 K to 77 K (Fig. 5e). This behavior is attributed to the reduced structural torsion and increased localization of the excited state at low temperatures.[29] On the other hand, the excited state of AIO compounds that follow the (M + X)LCT process leaves the structure relatively unperturbed.[69] Therefore, only little or no thermochromism has been observed on these AIO compounds, regardless of their dimensions (Fig. 5f). Further analysis on their time-resolved photoluminescence (TRPL) reveals more differences between these two different pathways. The PL lifetimes of the AIO compounds exhibiting CC emission show very little temperature dependence and are best fit with a single (first-order) exponential

decay function. Their average PL lifetimes are typically several microseconds (μs). Thus, the emission is attributed to phosphorescence, arising from spontaneous radiative decay from the lowest excited triplet state (T_1) to the ground state (Fig. 5d, top and Fig. 5e). In contrast, the decay times of the AIO compounds with (M + X)LCT emission show strong temperature dependance and can be best fit by a double exponential decay functions, indicating their emission arise from two different processes with comparable contributions, namely phosphorescence and thermally activated delayed fluorescence (TADF) (Fig. 5d, bottom and Fig. 5f). Upon cooling, the fraction of the short lifetime decay constant τ_1, which results primarily from TADF, drops significant from ~70% at 293 K to ~40% at 77 K.[29,30] This phenomenon has been observed previously in a number of Cu(I) based hybrid materials.[75–78] Due to the small energy barrier between the lowest excited singlet state (S_1) and T_1, a fraction of electrons can undergo reverse intersystem crossing (RISC) from T_1 back to S_1 and then follow radiative recombination from S_1 to S_0. Interestingly, while the emission energies and PL mechanisms are similar for μ^1-MC and μ^2-DC 1D-AIO structures, the latter generally have higher IQYs and can be twice as much as those of the former.[30] The difference in their emission efficiency is attributed to the difference in their coordination modes, and confirmed by the *ab initio* calculations and infrared (IR) spectroscopic studies. Compared to the μ^1-MC structures, the μ^2-DC structures show much stronger binding strength and significantly reduced ligand rotation and vibration, which gives rise to effectively supressed nonradiative decay and higher IQYs.

4. Applications of AIO compounds

4.1. Lighting phosphors for LEDs

Solid-state lighting (SSL) technology makes use of light-emitting diodes (LEDs) to convert electricity directly to light. Their color quality, durability and energy efficiency make them ideal for general lighting applications.[79] Currently white LED (WLED) technologies are primarily phosphor-converted WLEDs (pc-WLEDs), which are assembled by coating blue-excitable yellow or multicomponent phosphors onto blue LED chips to achieve overall white light.[80,81] For example, the benchmark yellow phosphor, cerium doped yttrium aluminum garnet (YAG: Ce^{3+}), emits intensive yellow light when excited by a blue LED. However, nearly all commercial phosphors currently used in pc-WLEDs rely heavily on rare-earth elements (REEs), which face potential supply and cost risks, as well as severe environmental consequences caused by their mining and extraction processes.[82–84] On the other hand, considering their high quantum yield, well tunable emission energy, robustness towards moisture and heat, and most importantly, low cost and easily scalable synthesis and solution processability, the AIO compounds may become a good candidate as alternative phosphors for clean energy lighting devices.

A number of AIO compounds having high IQYs and excellent blue excitability have been designed and synthesized. Among them, 1D-μ^2-Cu_4I_6(*5-m-bttmp*)$_2$ represents the best performing member. It emits bright orange color (λ_{em} = 596 nm) with IQY

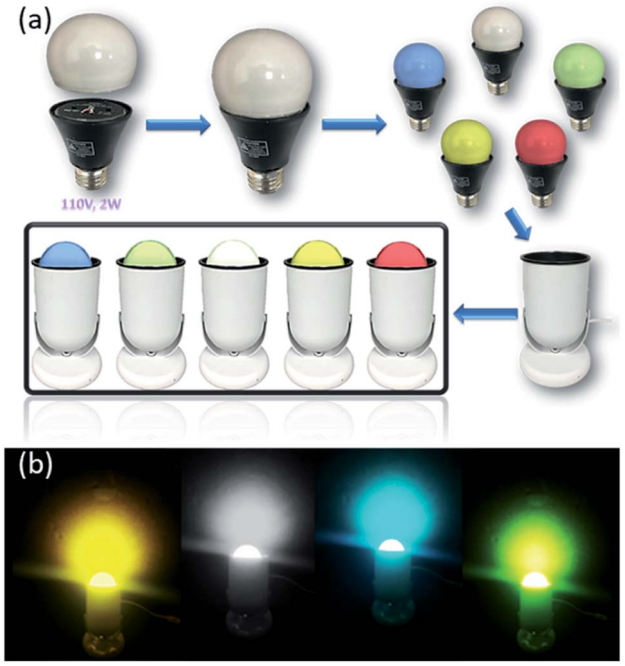

Fig. 6 (a) Schematic showing the assembly of prototype LED lighting devices based on AIO compounds. (b) Illuminating LED light bulbs (110 V, 2 W) coated by selected AIO-type phosphors. Reproduced with permission from ref. 29. Copyright 2020, American Chemical Society.

of 85% and 76% under UV (360 nm) and blue (450 nm) radiation, respectively.[30] Taking advantage of high solution processability of the AIO compounds, prototype LED bulbs using selected AIO compounds as phosphors have been assembled (Fig. 6a and b).[29] The phosphors are either in direct contact with the LED chips or are coated on the bulbs. UV or blue LED chips are used as excitation source for the phosphors.

4.2. Luminescent solar concentrators

Solar concentrators are used to provide higher optical concentration to solar cells in order to increase their electrical power. Conventional solar concentrators often use large mirrors to track the Sun and yield high optical intensities on solar cells at the focal point. However, they are expensive to deploy and maintain, and the process create undesirable heating effect on the solar cells.[85] An alternative to these devices that takes the advantages of high optical concentration without generating excess heat could be luminescent solar concentrators (LSCs).[86–88] LSCs are composed of a luminescent material dispersed in a highly transparent waveguide substrate. The sunlight is first absorbed by the luminescent material, then reemitted and gets directed to the solar cell at the sides by internal reflection (Fig. 7a).

Inspired by its unique properties, including large Stokes shift (114 nm), extremely high PLQY (>98%) and excellent solution-processibility, a 0D-AIO compound, Cu_4I_6(pr-ted)$_2$ has recently been investigated for possible use as a LSC material.[36] To evaluate its performance, a Cu_4I_6(pr-ted)$_2$/PVP (PVP = polyvinylpyrrolidone) ink was used to form a uniform and strongly

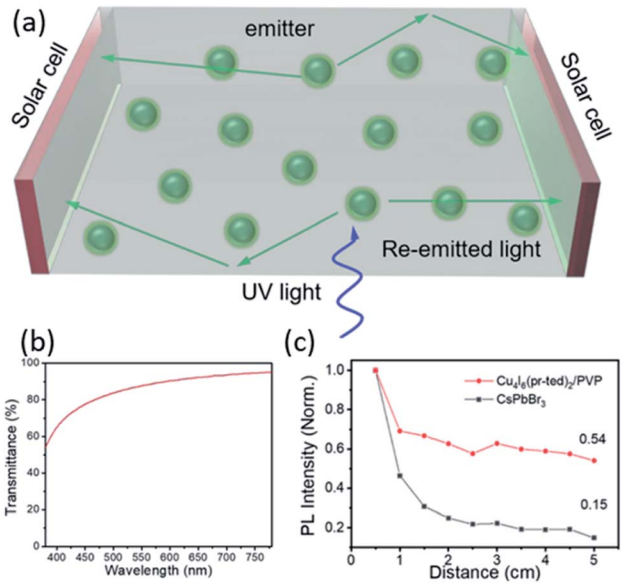

Fig. 7 (a) Schematic showing an LSC device using Cu_4I_6(*pr-ted*)$_2$/PVP ink. Green balls: Cu_4I_6(*pr-ted*)$_2$/PVP nanoparticles. (b) Light transmittance of prepared thin film in visible light region. (c) Comparison of PL intensities as a function of propagation lengths in the Cu_4I_6(*pr-ted*)$_2$/PVP film and $CsPbBr_3$ nanocrystal film. Reproduced with permission from ref. 36. Copyright 2020, American Chemical Society.

luminescent film on a large rectangular quartz substate (9 cm × 4.5 cm) by facile doctor-blade coating process. The optimized film maintains its PLQY as high as 76.1% and the average light transmittance in the visible light region is over 85% (Fig. 7b), while absorbing ultraviolet radiation strongly with an average UV light (365 nm) transmittance of less than 20%. These results suggest that the AIO-type materials are strong absorbers in high energy (UV) region and can be used as efficient energy converters.

In addition, one of the key limitations of LSCs is the significant luminescence reabsorption loss.[89] Thin films of $CsPbBr_3$ nanocrystals, a well-known perovskite structure with good solution-processibility and similar intensive green emission as the aforementioned AIO structure, Cu_4I_6(*pr-ted*)$_2$, were also prepared for comparison. Extinction coefficient (k) measurements conducted on both films reveal the fact that at their emission peaks, Cu_4I_6(*pr-ted*)$_2$/PVP exhibits much lower k value (0.024 at 529 nm) than $CsPbBr_3$ (0.64 at 520 nm). Since the lower k value, the smaller the reabsorption loss of the optical waveguide process, and the higher light utilization efficiency and better performance for LSC application,[90] Cu_4I_6(*pr-ted*)$_2$/PVP clearly demonstrates advantages than $CsPbBr_3$. This was further confirmed by the PL intensity as a function of propagation length of the light conduction in the films (Fig. 7c). The Cu_4I_6(pr-ted)$_2$/PVP film displays much slower PL intensity loss compared to the $CsPbBr_3$ film as the detection distance increased from 0.5 to 5.5 cm. The high PLQY, easy film processability and good waveguide property, coupled with the robustness towards heat and irradiation, making Cu_4I_6(pr-ted)$_2$ and similar AIO-type compounds as good candidates for LSCs.

5. Conclusions and outlook

As an interesting and emerging sub-class of copper halide based hybrid materials, AIO-type hybrid semiconductors represent an important addition to the advanced functional materials for clean-energy related applications. The modular nature of their structures, and the unique ionic/coordinate bonding at the inorganic and organic interface offer intriguing properties arising from the interplay of both components. These include: (1) high solubility in DMSO and other polar aprotic solvents, a desirable but rare feature for covalent/coordinate network materials, which grants solution-processed low-cost thin film fabrication desirable for many devices; (2) enhanced air, thermal and chemical stability as a result of forming stronger bonds between the inorganic and organic components; and (3) controllable tunability in binding mode, connectivity and crystal orbital energies making it possible to systematically tailor chemical and physical properties of these materials.

While applaudable progress has been made on the design and optimization of AIO-type CuX-based organic-inorganic hybrid semiconductors, some major challenges remain to be addressed and continued research and development are needed to further explore and optimize this material group. First of all, the efficiency of AIO based phosphors needs further improvement to meet the requirement for general lighting applications. The highest IQY achieved to date for the yellow-emitting AIO-type compounds is 76% under excitation of a blue light (450 nm) source, which is still significantly lower than REE-based commercial phosphors (>90%). Improving quantum efficiency may be achieved *via* efficient reduction of non-radiative decay by using more rigid ligands and/or forming chelating metal–ligand bonds to suppressed molecular motions. Secondly, current examples of higher dimensional AIO frameworks are sporadic and 3D AIO networks remain unidentified. By increasing the dimensionality of AIO structures, especially the inorganic backbones, it is expected that not only the framework stability but also optoelectronic properties in general (*e.g.* electrical conductivity, photoconductivity and carrier mobility), will be greatly improved, thus widening the range of their possible applications. Furthermore, current work on the AIO-type compounds is much limited on their photoluminescence properties. Investigations into electroluminescence, electrical and photoconductivity, carrier mobility and other properties relevant to LED and PV devices are important aspects of future research. Our most recent work on the fabrication of a prototype yellow LED using a robust AIO-type compound as the sole active emissive layer (EML) has yielded promising results and this will be a new direction in our future research. In addition, co-deposition with organic emitters as EMLs, a successful strategy that has been applied to neutral CuX hybrids,[91,92] will also be investigated as an alternative approach to achieve high performance AIO-based LED devices. Finally, the AIO approach may serve as a general and powerful tool for the design of other solution-processable and robust organic–inorganic hybrid material families. Although it has only been applied to CuX-based hybrid system at the present time, the structure-

building principles should be broadly applicable to many other materials, and we anticipate examples of AIO compounds in other semiconductor classes will emerge in the near future.

Conflicts of interest

There are no conflicts to declare.

Acknowledgements

The authors acknowledge the partial support from the U.S. Department of Energy, Office of Science, Office of Basic Energy Sciences (Grant No. DE-SC0019902).

Notes and references

1 X. Zhang, W. Liu, G. Z. Wei, D. Banerjee, Z. Hu and J. Li, *J. Am. Chem. Soc.*, 2014, **136**, 14230–14236.
2 H. Cho, S.-H. Jeong, M.-H. Park, Y.-H. Kim, C. Wolf, C.-L. Lee, J. H. Heo, A. Sadhanala, N. Myoung, S. Yoo, S. H. Im, R. H. Friend and T.-W. Lee, *Science*, 2015, **350**, 1222.
3 W. Liu, Y. Fang and J. Li, *Adv. Funct. Mater.*, 2018, **28**, 1705593.
4 M. D. Smith and H. I. Karunadasa, *Acc. Chem. Res.*, 2018, **51**, 619–627.
5 W. Liu, W. P. Lustig and J. Li, *EnergyChem*, 2019, **1**, 100008.
6 E. A. Dolgopolova and N. B. Shustova, *MRS Bull.*, 2016, **41**, 890–896.
7 J. Burschka, N. Pellet, S.-J. Moon, R. Humphry-Baker, P. Gao, M. K. Nazeeruddin and M. Grätzel, *Nature*, 2013, **499**, 316–319.
8 B. Saparov and D. B. Mitzi, *Chem. Rev.*, 2016, **116**, 4558–4596.
9 P. Gao, M. Grätzel and M. K. Nazeeruddin, *Energy Environ. Sci.*, 2014, **7**, 2448–2463.
10 L. Dou, Y. Yang, J. You, Z. Hong, W.-H. Chang, G. Li and Y. Yang, *Nat. Commun.*, 2014, **5**, 5404.
11 H. Wang and D. H. Kim, *Chem. Soc. Rev.*, 2017, **46**, 5204–5236.
12 Y. Zhao and K. Zhu, *Chem. Soc. Rev.*, 2016, **45**, 655–689.
13 B.-S. Zhu, Z. He, J.-S. Yao, C. Chen, K.-H. Wang, H.-B. Yao, J.-W. Liu and S.-H. Yu, *Adv. Opt. Mater.*, 2018, **6**, 1701029.
14 S. F. H. Correia, V. de Zea Bermudez, S. J. L. Ribeiro, P. S. André, R. A. S. Ferreira and L. D. Carlos, *J. Mater. Chem. A*, 2014, **2**, 5580–5596.
15 Y. Rong, Y. Hu, A. Mei, H. Tan, M. I. Saidaminov, S. I. Seok, M. D. McGehee, E. H. Sargent and H. Han, *Science*, 2018, **361**, eaat8235.
16 J.-P. Correa-Baena, M. Saliba, T. Buonassisi, M. Grätzel, A. Abate, W. Tress and A. Hagfeldt, *Science*, 2017, **358**, 739.
17 M. A. Green, A. Ho-Baillie and H. J. Snaith, *Nat. Photonics*, 2014, **8**, 506–514.
18 M. Grätzel, *Nat. Mater.*, 2014, **13**, 838–842.
19 N. J. Jeon, J. H. Noh, Y. C. Kim, W. S. Yang, S. Ryu and S. I. Seok, *Nat. Mater.*, 2014, **13**, 897–903.
20 A. K. Jena, A. Kulkarni and T. Miyasaka, *Chem. Rev.*, 2019, **119**, 3036–3103.
21 F. Huang, M. Li, P. Siffalovic, G. Cao and J. Tian, *Energy Environ. Sci.*, 2019, **12**, 518–549.
22 Y. Rong, Y. Ming, W. Ji, D. Li, A. Mei, Y. Hu and H. Han, *J. Phys. Chem. Lett.*, 2018, **9**, 2707–2713.
23 C. L. Raston and A. H. White, *J. Chem. Soc., Dalton Trans.*, 1976, 2153–2156.
24 R. Peng, M. Li and D. Li, *Coord. Chem. Rev.*, 2010, **254**, 1–18.
25 W. Liu, Y. Fang, G. Z. Wei, S. J. Teat, K. Xiong, Z. Hu, W. P. Lustig and J. Li, *J. Am. Chem. Soc.*, 2015, **137**, 9400–9408.
26 Y. Zhang, T. Wu, R. Liu, T. Dou, X. Bu and P. Feng, *Cryst. Growth Des.*, 2010, **10**, 2047–2049.
27 C. Chen, R.-H. Li, B.-S. Zhu, K.-H. Wang, J.-S. Yao, Y.-C. Yin, M.-M. Yao, H.-B. Yao and S.-H. Yu, *Angew. Chem., Int. Ed.*, 2018, **57**, 7106–7110.
28 T.-L. Yu, Y.-M. Guo, G.-X. Wu, X.-F. Yang, M. Xue, Y.-L. Fu and M.-S. Wang, *Coord. Chem. Rev.*, 2019, **397**, 91–111.
29 W. Liu, K. Zhu, S. J. Teat, G. Dey, Z. Shen, L. Wang, D. M. O'Carroll and J. Li, *J. Am. Chem. Soc.*, 2017, **139**, 9281–9290.
30 X. Hei, W. Liu, K. Zhu, S. J. Teat, S. Jensen, M. Li, D. M. O'Carroll, K. Wei, K. Tan, M. Cotlet, T. Thonhauser and J. Li, *J. Am. Chem. Soc.*, 2020, **142**, 4242–4253.
31 X. Hei, S. J. Teat, W. Liu and J. Li, *J. Mater. Chem. C*, 2020, **8**, 16790–16797.
32 A. V. Artem'ev, M. P. Davydova, X. Hei, M. I. Rakhmanova, D. G. Samsonenko, I. Y. Bagryanskaya, K. A. Brylev, V. P. Fedin, J.-S. Chen, M. Cotlet and J. Li, *Chem. Mater.*, 2020, **32**, 10708–10718.
33 R.-B. Zhang, J. Zhang, Z.-J. Li, J.-K. Cheng, Y.-Y. Qin and Y.-G. Yao, *Cryst. Growth Des.*, 2008, **8**, 3735–3744.
34 K. Tsuge, Y. Chishina, H. Hashiguchi, Y. Sasaki, M. Kato, S. Ishizaka and N. Kitamura, *Coord. Chem. Rev.*, 2016, **306**, 636–651.
35 A. V. Artem'ev, E. A. Pritchina, M. I. Rakhmanova, N. P. Gritsan, I. Y. Bagryanskaya, S. F. Malysheva and N. A. Belogorlova, *Dalton Trans.*, 2019, **48**, 2328–2337.
36 J.-J. Wang, C. Chen, W.-G. Chen, J.-S. Yao, J.-N. Yang, K.-H. Wang, Y.-C. Yin, M.-M. Yao, L.-Z. Feng, C. Ma, F.-J. Fan and H.-B. Yao, *J. Am. Chem. Soc.*, 2020, **142**, 3686–3690.
37 E. Cariati, E. Lucenti, C. Botta, U. Giovanella, D. Marinotto and S. Righetto, *Coord. Chem. Rev.*, 2016, **306**, 566–614.
38 V. W.-W. Yam, V. K.-M. Au and S. Y.-L. Leung, *Chem. Rev.*, 2015, **115**, 7589–7728.
39 Y. Fang, W. Liu, S. J. Teat, G. Dey, Z. Shen, L. An, D. Yu, L. Wang, D. M. O'Carroll and J. Li, *Adv. Funct. Mater.*, 2017, **27**, 1603444.
40 A. Bondi, *J. Phys. Chem.*, 1964, **68**, 441–451.
41 I. D. L. Albert, T. J. Marks and M. A. Ratner, *J. Am. Chem. Soc.*, 1997, **119**, 6575–6582.
42 Y. Slyvka, E. Goreshnik and M. Mys'kiv, *Chem. Met. Alloys*, 2017, 12–17, DOI: 10.30970/cma10.0351.
43 X. Gao, Q.-G. Zhai, S.-N. Li, R. Xia, H.-J. Xiang, Y.-C. Jiang and M.-C. Hu, *J. Solid State Chem.*, 2010, **183**, 1150–1158.
44 B. Tian, X. Zheng, T. J. Kempa, Y. Fang, N. Yu, G. Yu, J. Huang and C. M. Lieber, *Nature*, 2007, **449**, 885–889.

45 H. Morkoç, S. Strite, G. B. Gao, M. E. Lin, B. Sverdlov and M. Burns, *J. Appl. Phys.*, 1994, **76**, 1363–1398.
46 C. Szeles, *Phys. Status Solidi B*, 2004, **241**, 783–790.
47 P. Wang, Y. Wu, B. Cai, Q. Ma, X. Zheng and W.-H. Zhang, *Adv. Funct. Mater.*, 2019, **29**, 1807661.
48 J. Li, T. Inoshita, T. Ying, A. Ooishi, J. Kim and H. Hosono, *Adv. Mater.*, 2020, **32**, 2002945.
49 W. Nie, H. Tsai, R. Asadpour, J.-C. Blancon, A. J. Neukirch, G. Gupta, J. J. Crochet, M. Chhowalla, S. Tretiak, M. A. Alam, H.-L. Wang and A. D. Mohite, *Science*, 2015, **347**, 522.
50 K. Lin, J. Xing, L. N. Quan, F. P. G. de Arquer, X. Gong, J. Lu, L. Xie, W. Zhao, D. Zhang, C. Yan, W. Li, X. Liu, Y. Lu, J. Kirman, E. H. Sargent, Q. Xiong and Z. Wei, *Nature*, 2018, **562**, 245–248.
51 M. Singh, H. M. Haverinen, P. Dhagat and G. E. Jabbour, *Adv. Mater.*, 2010, **22**, 673–685.
52 N. Baroni, A. Turshatov, M. Adams, E. A. Dolgopolova, S. Schlisske, G. Hernandez-Sosa, C. Wöll, N. B. Shustova, B. S. Richards and I. A. Howard, *ACS Appl. Mater. Interfaces*, 2018, **10**, 25754–25762.
53 S. Allard, M. Forster, B. Souharce, H. Thiem and U. Scherf, *Angew. Chem., Int. Ed.*, 2008, **47**, 4070–4098.
54 C. B. Nielsen, S. Holliday, H.-Y. Chen, S. J. Cryer and I. McCulloch, *Acc. Chem. Res.*, 2015, **48**, 2803–2812.
55 J. M. Pietryga, Y.-S. Park, J. Lim, A. F. Fidler, W. K. Bae, S. Brovelli and V. I. Klimov, *Chem. Rev.*, 2016, **116**, 10513–10622.
56 Y. Shirasaki, G. J. Supran, M. G. Bawendi and V. Bulović, *Nat. Photonics*, 2013, **7**, 13–23.
57 M. Yuan, M. Liu and E. H. Sargent, *Nat. Energy*, 2016, **1**, 16016.
58 D. Liu, Y. Liu, P. Huang, C. Zhu, Z. Kang, J. Shu, M. Chen, X. Zhu, J. Guo, L. Zhuge, X. Bu, P. Feng and T. Wu, *Angew. Chem., Int. Ed.*, 2018, **57**, 5374–5378.
59 J. Zhang, X. Bu, P. Feng and T. Wu, *Acc. Chem. Res.*, 2020, **53**, 2261–2272.
60 Y. Fang, C. A. Sojdak, G. Dey, S. J. Teat, M. Li, M. Cotlet, K. Zhu, W. Liu, L. Wang, D. M. ÓCarroll and J. Li, *Chem. Sci.*, 2019, **10**, 5363–5372.
61 K. G. Stamplecoskie, J. S. Manser and P. V. Kamat, *Energy Environ. Sci.*, 2015, **8**, 208–215.
62 A. Sharenko, C. Mackeen, L. Jewell, F. Bridges and M. F. Toney, *Chem. Mater.*, 2017, **29**, 1315–1320.
63 Y. Guo, K. Shoyama, W. Sato, Y. Matsuo, K. Inoue, K. Harano, C. Liu, H. Tanaka and E. Nakamura, *J. Am. Chem. Soc.*, 2015, **137**, 15907–15914.
64 G. Schwarzenbach, *Helv. Chim. Acta*, 1952, **35**, 2344–2359.
65 P. C. Ford, E. Cariati and J. Bourassa, *Chem. Rev.*, 1999, **99**, 3625–3648.
66 M. Vitale* and P. C. Ford*, *Coord. Chem. Rev.*, 2001, **219–221**, 3–16.
67 S. Perruchas, X. F. Le Goff, S. Maron, I. Maurin, F. Guillen, A. Garcia, T. Gacoin and J.-P. Boilot, *J. Am. Chem. Soc.*, 2010, **132**, 10967–10969.
68 W. Liu, D. Banerjee, F. Lin and J. Li, *J. Mater. Chem. C*, 2019, **7**, 1484–1490.
69 Z. Liu, P. I. Djurovich, M. T. Whited and M. E. Thompson, *Inorg. Chem.*, 2012, **51**, 230–236.
70 Q. Benito, X. F. Le Goff, G. Nocton, A. Fargues, A. Garcia, A. Berhault, S. Kahlal, J.-Y. Saillard, C. Martineau, J. Trébosc, T. Gacoin, J.-P. Boilot and S. Perruchas, *Inorg. Chem.*, 2015, **54**, 4483–4494.
71 P. C. Ford and A. Vogler, *Acc. Chem. Res.*, 1993, **26**, 220–226.
72 K. R. Kyle, C. K. Ryu, P. C. Ford and J. A. DiBenedetto, *J. Am. Chem. Soc.*, 1991, **113**, 2954–2965.
73 C. K. Ryu, M. Vitale and P. C. Ford, *Inorg. Chem.*, 1993, **32**, 869–874.
74 S. Pramanik, C. Zheng, X. Zhang, T. J. Emge and J. Li, *J. Am. Chem. Soc.*, 2011, **133**, 4153–4155.
75 R. Czerwieniec, J. Yu and H. Yersin, *Inorg. Chem.*, 2011, **50**, 8293–8301.
76 M. J. Leitl, V. A. Krylova, P. I. Djurovich, M. E. Thompson and H. Yersin, *J. Am. Chem. Soc.*, 2014, **136**, 16032–16038.
77 T. Hofbeck, U. Monkowius and H. Yersin, *J. Am. Chem. Soc.*, 2015, **137**, 399–404.
78 R. Czerwieniec, M. J. Leitl, H. H. H. Homeier and H. Yersin, *Coord. Chem. Rev.*, 2016, **325**, 2–28.
79 S. Nakamura, *Science*, 1998, **281**, 956.
80 X. Huang, *Nat. Photonics*, 2014, **8**, 748–749.
81 Y. H. Kim, P. Arunkumar, S. H. Park, H. S. Yoon and W. B. Im, *Mater. Sci. Eng., B*, 2015, **193**, 4–12.
82 Q. Gong, Z. Hu, B. J. Deibert, T. J. Emge, S. J. Teat, D. Banerjee, B. Mussman, N. D. Rudd and J. Li, *J. Am. Chem. Soc.*, 2014, **136**, 16724–16727.
83 A. R. Chakhmouradian and F. Wall, *Elements*, 2012, **8**, 333–340.
84 T. Dutta, K.-H. Kim, M. Uchimiya, E. E. Kwon, B.-H. Jeon, A. Deep and S.-T. Yun, *Environ. Res.*, 2016, **150**, 182–190.
85 M. J. Currie, J. K. Mapel, T. D. Heidel, S. Goffri and M. A. Baldo, *Science*, 2008, **321**, 226.
86 M. G. Debije and P. P. C. Verbunt, *Adv. Energy Mater.*, 2012, **2**, 12–35.
87 F. Meinardi, A. Colombo, K. A. Velizhanin, R. Simonutti, M. Lorenzon, L. Beverina, R. Viswanatha, V. I. Klimov and S. Brovelli, *Nat. Photonics*, 2014, **8**, 392–399.
88 F. Meinardi, H. McDaniel, F. Carulli, A. Colombo, K. A. Velizhanin, N. S. Makarov, R. Simonutti, V. I. Klimov and S. Brovelli, *Nat. Nanotechnol.*, 2015, **10**, 878–885.
89 C. Tummeltshammer, A. Taylor, A. J. Kenyon and I. Papakonstantinou, *Sol. Energy Mater. Sol. Cells*, 2016, **144**, 40–47.
90 M. Abdel-Baki, F. A. Abdel-Wahab, A. Radi and F. El-Diasty, *J. Phys. Chem. Solids*, 2007, **68**, 1457–1470.
91 Z. Liu, M. F. Qayyum, C. Wu, M. T. Whited, P. I. Djurovich, K. O. Hodgson, B. Hedman, E. I. Solomon and M. E. Thompson, *J. Am. Chem. Soc.*, 2011, **133**, 3700–3703.
92 M. Xie, C. Han, Q. Liang, J. Zhang, G. Xie and H. Xu, *Sci. Adv.*, 2019, **5**, eaav9857.